Charles W. McCrackin, Henok G. Kiflu, Sarah E. Kruse, Philip E. van Beynen, Jason S. Polk and Ben. Miller. 3D resistivity survey over mapped caves in eogenetic karst terrane, west-central Florida, USA. *Journal of Cave and Karst Studies*, v. 84, no. 1, p. 1-13. DOI:10.4311/2017ES0125

3D RESISTIVITY SURVEY OVER MAPPED CAVES IN EOGENETIC KARST TERRANE, WEST-CENTRAL FLORIDA, USA

Charles W. McCrackin[1], Henok G. Kiflu[2], Sarah E. Kruse[2], Philip E. van Beynen[2], Jason S. Polk[3,C] and Ben. Miller[4]

Abstract

This study assesses the capability and practical applications of quasi-3 Dimensional (3D) Electrical Resistivity Tomography (ERT) for mapping air-filled conduits in eogenetic karst. A high-resolution quasi-3D ERT survey, consisting of multiple parallel 110m-long 2D profiles, was conducted over two mapped cave systems on the Brooksville Ridge, Florida. The irregularly shaped caves have diameters ranging up to 4 m and span depths from 3 m to 11 m below ground surface. Dipole-dipole array geometries with L_2 (least squares) rather than L_1 (robust) inversion produced the best fits of resistivity highs with the mapped cave locations. As expected, 3D inversions of sets of parallel lines produced better results than 2D inversions of individual transects. Better imaging was obtained of a cave over which cave-parallel profiles were run in addition to cross-cave profiles. However, even with the best acquisition and processing steps, there are significant misfits in the apparent size of the large cave sections, and narrower conduits are not imaged. Resolution decreased significantly with depth, as expected given the method limitations and the site constraints on profile lengths. 3D visualization techniques are explored, and found helpful in examining the data and comparing mapped caves and 3D resistivity datasets; however, when applied to eogenetic karst terrain, ERT has limited capacity to detect smaller cavities, which may require the additional use of other geophysical or subsurface investigative methods. With sinkholes continuing to be of concern to residential and urban development in west-central Florida, the results of this research present additional insight on the potential of quasi-3D ERT methods to map and characterize the potential hazards posed by karst terranes.

INTRODUCTION

Electrical Resistivity Tomography (ERT) can be an effective detection method for caves and voids in karst terrain (e.g., Doll et al., 1998; Schoor, 2002; Gibson et al., 2004; El-Qady et al., 2005; Leucci and De Giorgi, 2005; Parise and Gunn, 2007; Ezersky, 2008; Abu-Shariah, 2009; Pánek et al., 2010; Gambetta et al., 2011; Kaufmann et al., 2011; Zhu et al., 2011, McCormack et al., 2017; Prins et al., 2019). ERT methods are sensitive to the resistivity contrast between the host bedrock material and the void space. When caves exist in the vadose zone, the empty void space has a higher resistivity than the host rock. In the phreatic zone, water-filled cavities generally appear as resistivity lows against the host rock background (Zhu et al., 2011; Land et al., 2012; Gary et al., 2013; Redhaounia et al., 2016; Majzoub et al., 2017; Nazaruddin et al., 2017; Redhaounia et al., 2017).

The use of geophysical techniques for void detection was pioneered in telogenetic karst settings (Crawford, 1989; Crawford et al., 1999), where the rock has undergone diagenesis and compaction, and the porosity is often low, with voids existing in long, linear pathways following joints or bedding planes (Palmer, 2007). Such terranes include much of the southeastern and central United States. In contrast, eogenetic karst regions, such as Florida and much of the carbonate islands of the Caribbean, contain geologically young limestones having high primary porosity and matrix permeability (Vacher and Mylroie, 2002). Voids in eogenetic karst systems present challenges to detection, compared to the extensive cylindrical voids that may form in mature karst. In eogenetic karst, both high primary porosity (Vacher and Mylroie, 2002) and a tendency of voids to fill with sediments (Jenson et al., 2006) act to reduce the resistivity contrast between caves and rock. Caves tend to be smaller and may be more complex in geometry due to the higher permeability bedrock and dominance of matrix flow overprinting structural controls that tend to guide void detection in telogenetic karst areas (Florea, 2006; Palmer, 2007). Both vertical shafts and horizontal voids are expected from varied processes near the surface and near the water table (Jenson et al., 2006). Nevertheless, detecting voids in young carbonate karst systems (eogenetic limestones) is increasingly important as a tool for mapping the potentiometric surface, petroleum extraction, and salt water intrusion threats (Lace and Mylroie, 2013).

With the advent of automated multi-electrode resistivity array systems, resistivity survey times have significantly decreased and have allowed for greater amounts of data to be collected. This has led to the more frequent use of two-dimensional (2D) and now three-dimensional (3D) ERT imaging (Loke et al., 2013). Traditional 2D ERT surveys

[1] Rimkus Consulting Group, Inc.
[2] University of South Florida
[3] Western Kentucky University
[4] United States Geological Survey
[C]Corresponding Author: jason.polk@wku.edu

have proven successful in the detection of various 3D features when these features are large compared to the electrode spacing. Examples of such features include sinkholes (Schoor, 2002; Kruse et al., 2006; Margiotta et al., 2012), landslides (Schrott and Sass, 2008; Pánek et al. 2010; Zhou and Beck, 2011), and caves (Leucci and De Giorgi, 2005; El-Qady, 2005; Abu-Shariah, 2009; Gambetta et al., 2011: Kaufmann et al., 2011); however, 2D ERT may not always be appropriate for mapping complex geology (Loke and Barker, 1996b; Roth et al., 2002; Zhu et al., 2011). A 3D survey may be best suited, particularly when a volumetric approach is required or when resolution of geometric detail is desired, as in archeological surveys (Loke and Barker, 1996b; Roth et al., 2002; Papadopoulos et al., 2006; Neyamadpour et al., 2010; Chambers et al., 2012). Additionally, 2D ERT surveys can suffer from artifacts generated by off-line 3D features in complex environments such as might be expected in eogenetic karst (Roth et al., 2002; Gharibi and Bentley, 2005; Martorana et al., 2009; Zhu et al., 2011).

With true 3D arrays, many varieties of array geometries are possible. Currently, most 3D resistivity surveys are quasi-3D surveys, in which data are collected along sets of parallel linear profiles with classic 2D geometries. Parallel profiles are then inverted as a 3D block unit. This process can be repeated with orthogonal line sets (Papadopoulos et al., 2006; Papadopoulos et al., 2010; Rucker et al., 2009; Neyamadpour et al., 2010; Chambers et al., 2012;).

Such quasi-3D geometries have been applied to image complex geologic structures in a variety of terrains (Loke and Barker, 1996b; Gharibi and Bentley, 2005; Neyamadpour et al., 2010; Kaufmann et al., 2012; Mohamed et al., 2019; Fu et al., 2020; Torrese, 2020), but have not, to our knowledge, been described in shallow, thinly mantled eogenetic karst terranes. The foci of this study are to assess surveying and modeling strategies using the quasi-3D ERT method. The study utilizes currently available commercial systems and software to examine the practical limitations of the method for detecting voids in eogenetic karst terranes.

REGIONAL GEOLOGY

The ~100 m by 110 m study site is situated on the Brooksville Ridge of West-central Florida and within the Withlacoochee State Forest of Citrus County (Fig. 1). The Brooksville Ridge is an upland area of west-central Florida, which hosts dozens of air-filled caves and cover collapse sinkholes (Florea, 2006; Harley, 2007; Pace-Graczyk, 2007; Polk, 2009). The larger southern portion of the Brooksville Ridge, where the study area is located, is approximately 175 kilometers in length and varies from 15 kilometers to 100 kilometers in width. The ridge trends in a NW to SE direction and is parallel to the western edge of Florida's coastline. The elevation of the Brooksville Ridge ranges from 20 meters to 60 meters with irregular areas of limestone outcrops (White, 1970).

Figure 1. Location of Bottle Cap and Legend Caves on the Florida Peninsula.

The site was selected because it overlies two well-documented vadose caves, Legend Cave (Fig. 2) and Bottle Cap Cave (Fig. 3). Such caves are common features on the Brooksville Ridge, where changes in sea level have contributed to the formation of many vadose zone cavities (Sinclair et al., 1985; Brinkmann and Reeder, 1994; Florea, 2006). Many of these caves are characterized by a distinctive keyhole or diamond shape appearance that is a result of groundwater elevation responding to sea level fluctuations. Present day sea level is now approximately 30 meters to 45 meters lower than the Late Eocene time period (Lane, 1994). The vadose zone caves of the Brooksville Ridge are thought to have formed during periods of stability of Quaternary sea levels (Florea et al., 2007) although some passages in the caves do not adhere to this theory.

A strong correlation between Florida cave levels and marine terraces has been reported, suggesting a tiered system of subaerial caves on the Brooksville Ridge (Florea et al., 2007). Changes in sea level have significantly influenced the topography and the formation of caves in the state of Florida as indicated by the Marine Terraces and Shoreline of Florida Map (Healy, 1975). The two caves imaged in this study are located between the Wicomico and Penholoway terrace. The contact between the Wicomico and Penholoway terrace is at an elevation of approximately 21 meters, which corresponds with the elevation of the study area. Many of the cave passages on the Brooksville have been reported as similar in architecture and characterized by laterally extensive, air-filled cavities with bedrock pillars, dissolution features, and passages that often terminate in blind pockets (Florea, 2006). The groundwater table for this area is below a depth of 16 meters. Cave passages in the ridge generally are known to trend along a NE to SW and NW to SE system of fractures.

In this region, a thin veneer of Miocene (5 Ma to 23 Ma) siliciclastic sands and clays (Hawthorn Group) overlie highly karstified Suwannee Limestone, which, in turn, unconformably overlies the eogenetic Ocala Limestone (Scott, 2001). Outcrops of Oligocene Suwannee Limestone consist of dolostone to dolomitic limestone that is highly silicified with chert lenses. Where the Suwannee Limestone has been eroded away, the underlying Ocala Limestone can be found at the surface. This Late Eocene Ocala Limestone underlies most of Florida and is a soft, highly porous and permeable limestone, but can locally be less porous and permeable, because of the cementation by crystalline calcite (FGS, 2010). Numerous disappearing streams and springs are associated with the Ocala Limestone. At the surface, exposures of the Ocala limestone reveal caverns and solution pipes that result from intense karstification (Sinclair et al., 1985; Florea, 2006) and often develop into voids eventually leading to the formation of cover collapse sinkholes. Together, these limestone units form part of the intermediate confining unit of the Florida Aquifer System (Scott, 2001; FGS, 2010). In areas where Hawthorn deposits exist, the Hawthorn provides a cap of protection from dissolution, and directs water off the mixed sand and phosphatic clays into subsurface conduits, whereby cave development often occurs in the first 10−30 meters of bedrock (Polk et al., 2012). This is primarily due to the highly permeable (up to 10^{-6} m s^{-1}) rock, which can have an initial porosity of nearly 30 percent or more (Florea and Vacher, 2006).

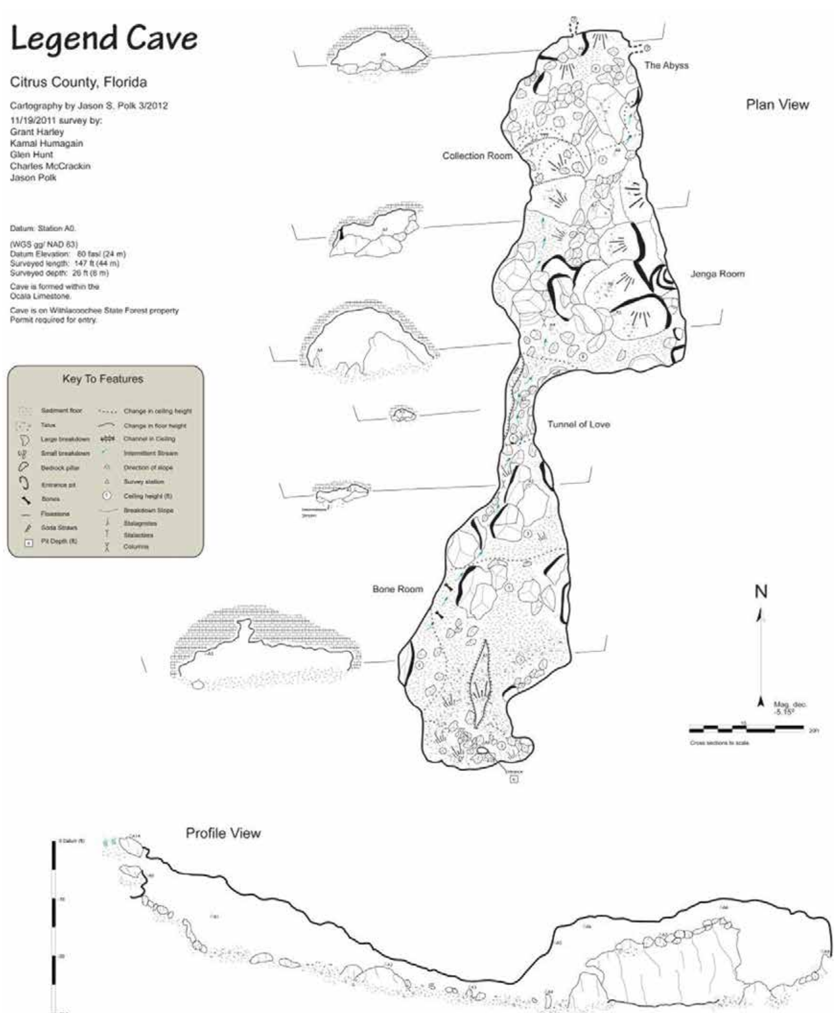

Figure 2. Map of Legend Cave, Citrus County, Florida (Polk, unpublished).

STUDY SITE

At the study site, resistivity profiles were performed over Legend Cave (Fig. 2) and Bottlecap Cave (Fig. 3). Their entrances are ~100 m apart and separated by a limestone quarry pit approximately 20 m in diameter

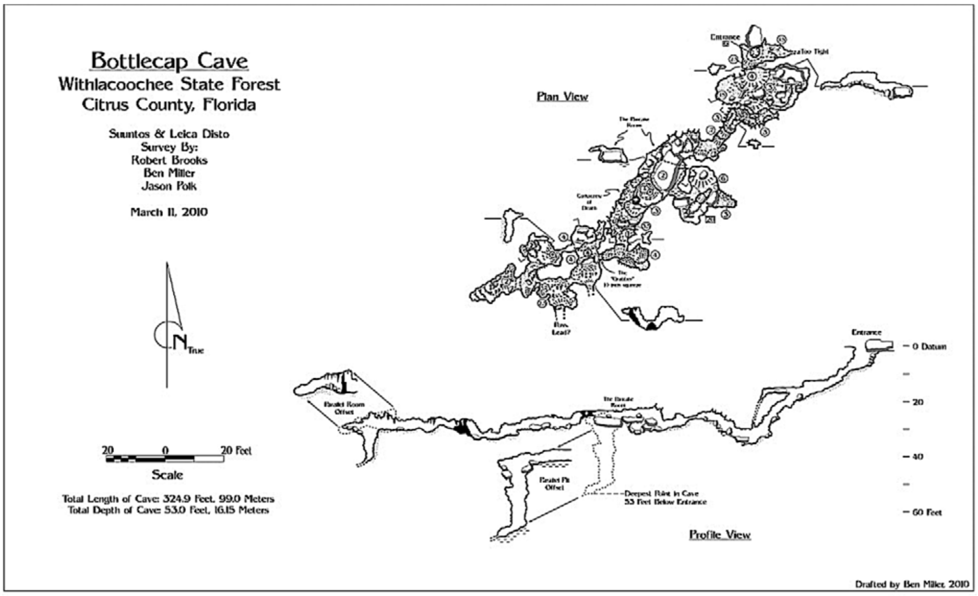

Figure 3. Map of Bottlecap Cave, Citrus County, Florida.

and approximately 3 m to 7 m in depth. The limestone quarry has a water table that is perched for most of the year. The quarry is underlain by organic and clayey soils that overlie the siliceous Suwannee Limestone.

The entrance to Legend Cave is located at the southeast corner of the quarry pit and the cave trends in a N−S direction at the eastern boundary of the site. A detailed cave survey measured a depth of approximately 3 m to 9 m below land surface and a length of 44 m (Fig. 2). Legend Cave consists of three large rooms separated by two narrow, collapsed passages located at the central and north-central portions of the cave. Considerable breakdown from roof collapse and infilling of sediments are readily visible. Roof collapse has blocked the far north end of the cave and prevented further exploration.

Bottlecap Cave trends in a NE−SW direction with an entrance at the northwest portion of the site. This cave is characterized by small circular conduits. Cave depth ranges from 6 m to 11 m below the surface with a surveyed length of 107 m (Fig. 3). A dry vertical shaft that extends to a depth of approximately 18 m below datum is the deepest part of the cave. No groundwater is present in either cave.

The geometries of both Bottlecap and Legend Cave suggest relatively simple linear structures, which have undergone extensive dissolution, collapse, and partial sediment in-filling. Cave development occurred during past periods of higher sea levels and groundwater flow. Currently, meteoric waters are washing the clayey Hawthorn sediments into the caves, with thicker sediments at the entrances and subsequent thinning of sediments further into the caves. Large limestone blocks from roof collapse prevent the exact identification of the lowest levels of the caves. Cave walls are often irregular due to extensive breakdown of the eogenetic bedrock, and thus, unclear structural controls on localized passage development. Although the limestone surface in the caves is generally dry, various zones of saturated rock were observed along fractures in the roof and walls. Variable topography, irregular limestone surfaces and passage development, and infilling of sediments in the relatively simple caves present a complex subsurface geology for geophysical imaging, and clearly limits precise delineation of the cave's true extent. Most notably, collapse structures at the ends of the caves suggest potential inaccessible voids.

ARRAY GEOMETRY

For the quasi-3D process, the user runs a series of parallel 2D profiles. In this study, we sought to select from 2D array geometries that are available, pre-programmed by commercial software or hardware manufacturers, and thus readily used by practitioners in the field. The broader field of optimal selection of arbitrary combinations of readings is a topic of current research, but the capacity to generate specifically optimized arrays remains beyond the reach of the typical end-user at present (Loke et al., 2013). Pre-programmed 2D arrays typically available are the Dipole-Dipole, Wenner, and Inverse-Schlumberger arrays (Fig. 4). Selecting the most appropriate array type depends on survey goals, site geology, and structure of the feature being surveyed (Dahlin and Zhou, 2004).

Each of these arrays has previously been used for cavity detection (Gharibi and Bentley, 2005; Neyamadpour et al., 2010; Pánek et al., 2010). The Wenner and Inverse Schlumberger arrays have a higher signal to noise ratio and a deeper depth of investigation compared to other arrays (Dahlin and Zhou, 2004; ASTM D 6431-99). We note the Inverse-Schlumberger array mimics a traditional Schlumberger array, but with the roles of outer current and inner potential electrodes switched to outer potential and inner current (Fig. 4). Many multi-electrode resistivity systems are now available in a mode such that, potential differences between multiple pairs of electrodes can be measured and recorded simultaneously. The Wenner array geometry cannot exploit the capability of such multi-channel systems so acquisition is slower per potential-current pair combination than for other geometries. Dipole-Dipole surveys in particular yield a high number of measurements in the near-surface and offer good horizontal resolution, and are thus well suited for

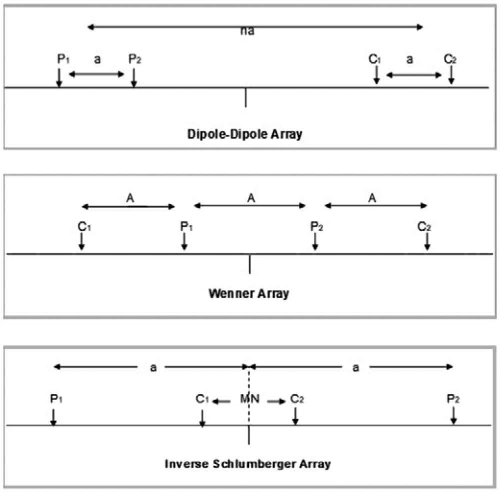

Figure 4. Dipole-Dipole, Wenner, and Inverse Schlumberger array type.

mapping complex structures (Dahlin and Zhou, 2004). The Dipole-Dipole geometry can also provide better resolution of higher resistive anomalies (Martorana et al., 2009; Pánek et al., 2010). As a result, the Dipole-Dipole array has proven to be one of the more effective array types for cavity detection (Cardarelli et al., 2010; Neyamadpour et al., 2010; Kaufmann et al., 2011); however, the Dipole-Dipole array suffers from a lower signal to noise ratio (Dahlin and Zhou, 2004; Gharibi and Bentley, 2005) and is especially susceptible to near-surface artifacts from electrode spacing errors, thus combining it with a strong-gradient array may improve the ability to resolve irregularities in the subsurface.

In this case study, in which lateral variability (the presence of caves) is our primary target, we consider the relative value of Dipole-Dipole and Inverse Schlumberger measurements and their combination. The slower Wenner arrays with lower lateral resolution were not acquired.

In addition to the type of array(s) selected, consideration of array orientation and electrode spacing is critical to image quality (Jackson et al., 2001; Gharibi and Bentley, 2005; Abu-Shariah, 2009; Pánek et al., 2010; Cardarelli et al., 2010; Zhu et al., 2011; Leucci et al., 2016). For the interpretation of a single profile over an elongated cave, it is clearly desirable to orient the profile perpendicular to the cave. The optimal orientation for quasi-3D approach, however, will depend on target shapes. Gharibi and Bentley (2005) suggest that closely spaced transect lines in one direction may be more beneficial than orthogonal transects with a larger electrode spacing.

Optimal Inversion Methods

Once the readings are acquired, the terrain resistivity is determined by inverting the raw data for the best-fitting underlying structure. The definition of best-fit typically falls into one of two categories: an L_2-norm (Least-Squares or Smooth) inversion in which a weighted mean square error (between readings and model predications) is minimized, and an L_1-norm (Robust) inversion in which a weighted mean absolute error is minimized (Loke and Barker, 1996a; Dahlin and Zhou, 2004; Gharibi and Bentley, 2005; Catt et al., 2009; Cardarelli et al., 2010). While both methods have been successfully used to resolve cavities, selecting the most appropriate inversion depends largely on the target type, target geometry, (Dahlin and Zhou, 2004; Catt et al., 2009) and the amount of noise in the dataset (Catt et al., 2009). With constraints on the smoothness of the model, the L_2-norm inversion has been more commonly used (Loke and Barker, 1996; Jackson et al., 2001; Roth et al., 2002; Gharibi and Bentley 2005; Papadopoulos et al., 2006; Cardarelli et al., 2010, Zhu et al., 2011), although its inability to accurately resolve the position of geologic boundaries has been noted (Chambers et al., 2012). When mapping complex and abrupt geologic boundaries, the L_1-norm (Robust) inversion, has been described as the more accurate of the two methods (Dahlin and Zhou 2004; Neyamadpour et al., 2009; Neyamadpour et al., 2010; Chambers et al., 2012). These studies also show that robust inversion works well with noisier data sets and may help to resolve 3D structures when lateral variations are more frequent. The two inversion methods are compared in this case study.

METHODS

Cave Mapping

Each of the caves in this study area was mapped to the Union Internationale de Spéléogie UIS “UISv1 5-4-B” survey grade with an expected overall accuracy of two percent (Häuselmann, 2010). A UIS Grade 5 level survey requires measurement length to be within 0.05 m of error, as well as compass (declination corrected) and clinometer readings to the nearest degree (Häuselmann, 2010). Surveys used frontsight and backsight measurements of passage distances, inclinations, and azimuths, and all loops were closed and adjusted. The precision total length was within 0.05 m and the compass and clinometer readings within one degree of accuracy. Final survey data reduction was completed using COMPASS cave software to produce lineplots that were converted to 3D shapefiles and exported for 3D modeling via ArcGIS and used for final map drafting of features, which was completed in Adobe Illustrator (Legend Cave) and Xara (Bottlecap Cave) software (Kambesis et al. 2015). Both the surveyed length and total length measurements were used as appropriate in correcting for the 3D ERT survey. ArcGIS was used to georeference the cave entrances and passages relative to the ERT survey (Kambesis et al. 2015).

3D models of Legend and Bottlecap Caves were created using the plan and cross-sectional views from each of the cave maps using AutoCAD Civil 3D and Meshlab. These models are simplified versions of the cave geometry, designed to capture the major cave dimensions with an accuracy of ~0.5−1 m. This accuracy is higher than the typical spatial resolution of the resistivity inversions at comparable depths, so is deemed sufficient for comparison of the cave locations and the resistivity data.

Site Delineation

A fence along the access road was used as the baseline from which each ERT transect was measured. Survey boundaries and ERT transect endpoints were established using a Total Station GPS and locations were collected at the site boundaries to identify coordinates for georeferencing and positioning relative to georeferencing aerial imagery and LiDAR data.

A topographic map was created from the Citrus County LiDAR data obtained from the Southwest Florida Water Management District, which has vertical resolution of ~0.3 m (SWFWMD, 2006). The topographic data were used to generate a terrain correction for the ERT survey. Topographic relief is approximately 9 meters across the site.

Survey Design

A 2D synthetic model was created to determine the optimum transect layout prior to surveying (Jackson, et al, 2001; Abu-Shariah, 2009; Catt et al., 2009). Based on the cave depths and the forward model results, a linear array of 56 electrodes was selected with an electrode spacing of 2 meters, which was a compromise between spatial resolution and depth of investigation. With a total line length of 110 meters, resistivity resolution below the cave depths was expected along the central portion of each profile. Parallel 2D transects were collected and spaced 4 meters apart so as not to exceed 2 times the electrode spacing (Gharibi and Bentley, 2005). The quarry pond and limestone outcrops prohibited acquisition in the southeast section of the site, and access prohibited data acquisition beyond the southern and eastern site boundaries and hence optimal resolution of Legend Cave. In total, there were 31 ERT transects with their direction and path selected for accessibility and to optimize coverage over the two known cave systems (Fig. 5a). On each profile, both the Dipole-Dipole and Inverse Schlumberger data sets were acquired.

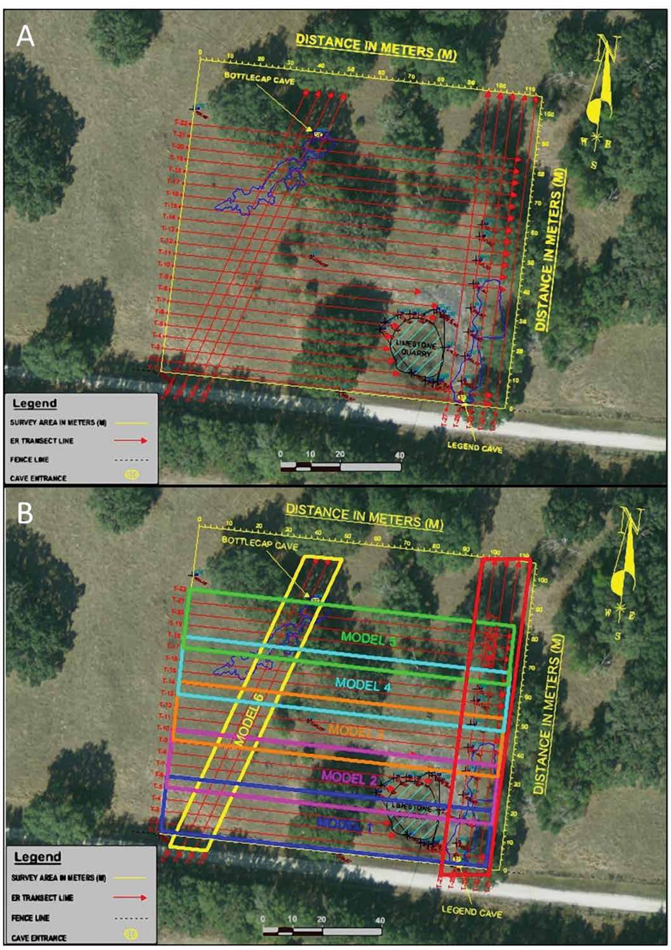

Figure 5. (a) View of the survey area with twenty-two (22) ER transects performed in a west to east direction which trended from the south of Legend Cave to the north of Bottlecap Cave. Additionally, four (4) orthogonal transects were performed over the approximate centerline of Bottlecap Cave and five (5) orthogonal transects were performed over Legend Cave; (b) diagram showing the 7 models which were individually processed, terrain corrected, and imported into a larger 3D data set.

Resistivity Data Processing

Measurements for each of the ERT transects were processed and terrain corrected with EarthImager software 2D version 2.4.0 and 3D version 1.5.4 (32-bit). Outlying data points that had a relative data misfit greater than 40 percent to the inverse model predictions after 6 iterations were deleted. In general, data with a relative misfit of 50 percent or greater is considered poorly fit and should be removed (AGI, 2009). Fewer than five percent of the data points were selected for removal. Selected profiles were then inverted individually with 2D inversions. Profiles were then inverted with EarthImager's 3D inversion algorithm in batches of up to six adjacent profiles (Fig. 5b).

Computer memory limitations precluded a full 3D inversion of larger subsets of the data. This is a significant limitation of the method and has been previously noted (Rucker et al., 2009). Both 2D and 3D inversions were run for various combinations of data and inversion parameters, including Dipole-Dipole and Inverse Schlumberger and combination arrays, L_1-norm and L2-norm error criteria, various convergence criteria to terminate iterations, and various smoothing criteria. Finally, results of 2D and 3D inversions were compared to slices through or volumes of the mapped cave positions. 2D plotting was done with EarthImager, 3D plotting was completed with EarthImager 3D and imported into Voxler 3D. Other forms of data processing, including 3D gridding of inverted resistivity data, may have assisted in generating void volume representations.

RESULTS AND ANALYSIS

Array Geometries

To assess the relative effectiveness of the Dipole-Dipole and Inverse Schlumberger array geometries, 2D inversion results for Transect 29 were compared against known cave position. Transect 29 closely tracks the centerline of Legend Cave, as shown in Figure 6a. For this test, the L_2-norm with EarthImager default inversion parameters were used. None of the 2D arrays properly captures information about the base of the cave, but the Dipole-Dipole and merged Dipole-Dipole and Inverse Schlumberger arrays show much more pronounced resistivity contrasts associated with the top of the northern section of the cave. The images generated from all three geometries show a distinctive shallow resistivity high to the north of the mapped caves (Fig. 6a). This feature is persistent in the data regardless of inversion method, and is discussed further below. For 3D inversions (of the data blocks as shown in Figs. 7 and 8) similar analysis showed that the Dipole-Dipole data gave subjectively better fits to the cave geometries.

2D vs. 3D Resistivity

3D inversions should theoretically yield improved matches between resistivity highs and mapped cave locations. Our data suggest this is generally the case at the study site. A 3D inversion profile was extracted from a block inversion consisting of three transects (Transects 28 thru 30). For comparison, 2D and 3D results are generated with L_2-norm EarthImager default criteria (Fig. 6b). Figure 6b shows the 2D inversion of the single central profile of T29 over Legend Cave in comparison to the central transect extracted from the 3D inversion block. Although the 2D result better fits the top of the northern portion of the cave, the 3D inversion better recovers the bottom and general structure of Legend Cave. We unfortunately have no direct observations to assess differences between the 2D and 3D models in the very near surface.

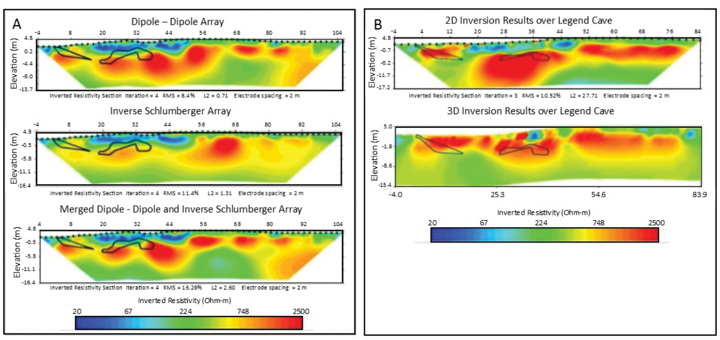

Figure 6. (a) 2D analysis of profile T29 (location shown on Figure 3) with different array geometries. The Dipole-Dipole and merged array geometries show a stronger resistivity contrast associated with the top of the cave; (b) comparison of 2D and 3D inversion profiles over the center of Legend Cave using the Dipole-Dipole array and L_2-norm inversion criteria

Figure 7 illustrates another example of differences between 2D and 3D inversions in this heterogeneous setting. Here profiles are compared which run along the southern boundary of the site that do not span a mapped cave feature. A 2D inversion of profile T2 indicates an apparent anomaly that is absent in a 3D inversion of profiles T1−T3.

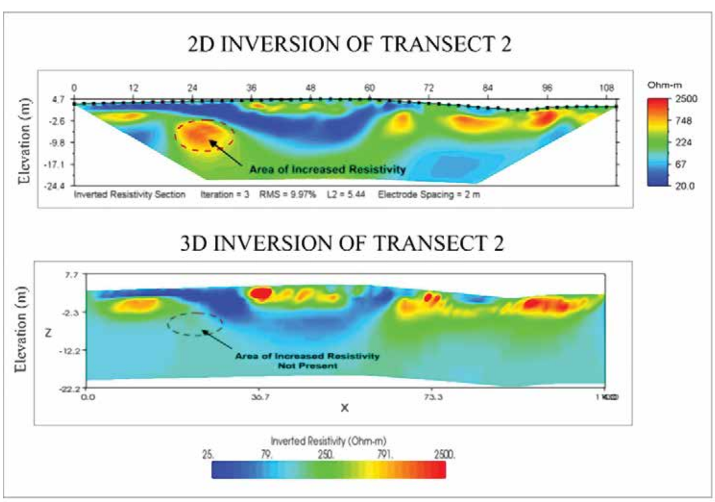

Figure 7. 2D inversion along Transect 2 indicates an isolated area of increased resistivity at 24 meters along the transect line, in comparison; 3D combined inversion of transects 1−3 shows no anomaly.

L_1-norm and L_2-norm Inversion Methods

We compared results from the L_1-norm and L_2-norm inversions at this study site. Figure 8 shows the two inversion types for the 3D grouping of four north-south profiles that traverse Legend Cave. For this study, the L_2-norm inversion yields a better fit in that it shows a resistivity high at the northern segment of Legend Cave. Overall, the L_2-norm smooth inversion was determined to be the method that better reproduced known features and was used for the 3D block results described below. It is important to note that others have reported best results with the L_1-norm robust inversion method (Loke and Barker, 1996a; Dahlin and Zhou, 2004; Gharibi and Bentley, 2005; Catt et al., 2009; Cardarelli et al., 2010). This may be related to site conditions, which are particularly heterogeneous in terms of host rock resistivity and the geometry of the target.

Profile Orientation

To assess whether it is preferable to run transect lines parallel or perpendicular to elongated cave features, we compared the central profile of the 3D block consisting of transects T17−T22, Model 5 trending in an E−W direction, and perpendicular to the Bottlecap Cave (Figure 9a) against the central profile of a 3D block consisting of transections T32−

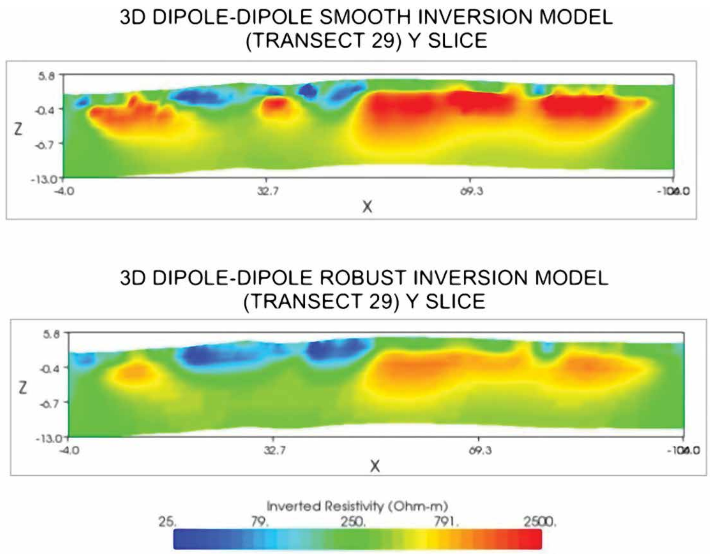

Figure 8. A comparison of the L_2-norm (smooth) inversion and the L_1-norm (robust) inversion. The profile was extracted along T29 from the 3D block model using profiles T28−T31 over Legend Cave (see Figure 3 for location).

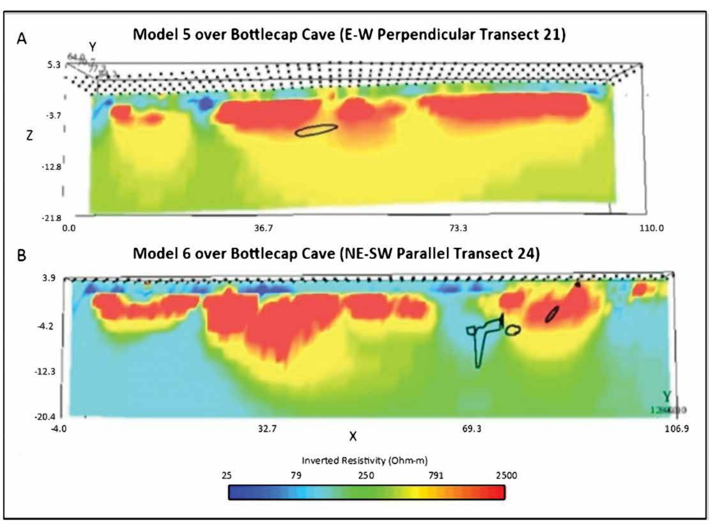

Figure 9. (a) Profile extracted from Model 5 over Bottlecap Cave (see Figure 8 for location). Black line shows projected geometry of Bottlecap Cave under T21. Contour interval ranging from 25–2,500 Ωm; (b) Profile extracted from Model 6 over Bottlecap Cave (see Figure 8 for location). Black line shows projected geometry of Bottlecap Cave under T21. Contour interval ranging from 25–2,500 Ωm.

T35, Model 6 trending in an NE−SW direction, and parallel to Bottlecap Cave (Fig. 9b). The first block, labeled Model 5 in Figure 9a, was created from E−W electrode arrays set at an angle of ~60 degrees to the long axis of Bottlecap Cave. In the second block, labeled as Model 6 in Figure 9b, the NE−SW electrode arrays are set more closely parallel, at an angle of ~20 degrees to the long axis of Bottlecap Cave (Fig. 10).

The results are inconclusive, as neither dataset showed agreement with the mapped cave passage location. In Model 6, we note an increase in resistivity corresponding with the entrance to Bottlecap Cave; however, where a vertical increase in the cave height exists, a discontinuity and low resistivity response are observed. Similarly, in Model 5, the known cave feature lies below a zone of resistivity highs. We note that Transect 24 is off-line from the center of Bottlecap Cave and that the cave passages consist of small diameters and highly complex morphology.

Comparatively, we note that on the 3D models discussed below there is generally better resolution of Legend Cave from profiles that are more closely parallel to the cave than there is for Bottlecap Cave, where profiles are more oblique to the centerline of the cave.

Analysis of cross-over points and model statistics of the resistivity values show a higher increase in resistivity over cave areas in the E−W transects than in the N−S transects. At crossings, perpendicular transects may show significantly different resistivities for the same material at similar depths. These cross-over errors range from 50 Ωm to 8,000 Ωm and indicate that the uncertainties associated with the resistivity values derived from the 2D transects are quite large in this highly variable 3D environment. This high variability illustrates the inherent geomorphologic heterogeneity and structural complexity of this karst landscape.

3D Block Models

In total, seven 3D block models were generated and then terrain corrected (Fig. 8). Three of the models shown here were derived from the Dipole-Dipole array and inverted using the Smooth inversion method (Fig. 8). A large increase in resistivity was observed on the north side of Legend Cave, which is cut off by roof collapse.

Figure 10a shows a resistivity low just north of the limestone quarry pit, which could possibly indicate an out-of-plane effect of the water-filled pit. An isolated resistivity high coincides with limestone outcrops. The northernmost extent of Legend Cave is not apparent in the eastern edge of the resistivity grid, presumably due to lack of depth resolution at the edge of the grid.

Taken together, the seven 3D Dipole-Dipole Models showed some correlations between resistivity highs and the sites of the two known cave systems. Bottlecap Cave, with depths centered approximately 8.5 meters below land surface, generally coincides with resistivity highs as seen in Figure 10b. Legend Cave, 3 meters to 9 meters below datum, conforms generally in length and depth with resistivity highs in the block model that is aligned with the cave (Fig. 10c), but there are significant mismatches in details of the shapes of the voids (Fig. 10b).

There are numerous zones of high resistivity in the inversions that are similar in size, shape, and depth of the two known cave systems at the site (Figs. 10b-c). The resistivity data suggest that significant unmapped void features may

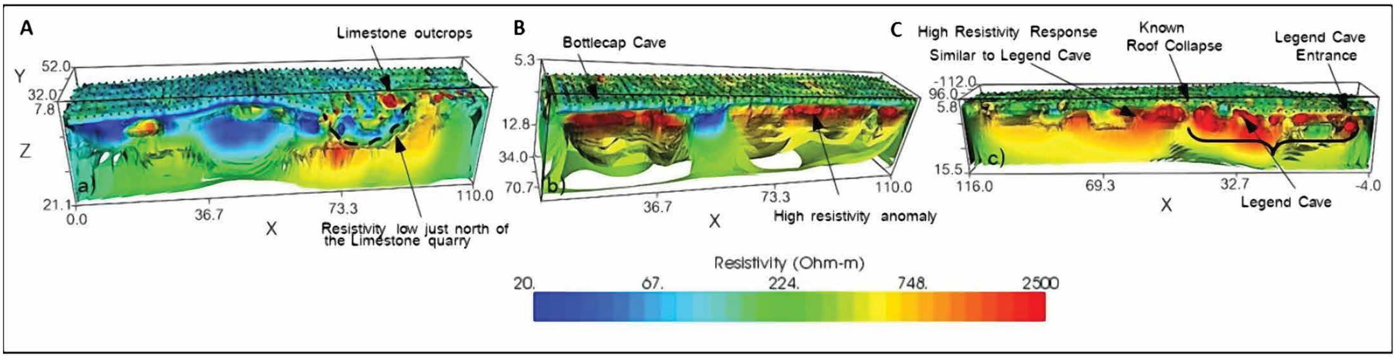

Figure 10. (a) A view of Model 3 facing North. See orange box on Figure 8 for location. Note the resistivity low that appears just north of the edge of the limestone quarry pit; (b) A view of Model 5 facing North. See green box on Figure 3b for location. Note the multiple high resistivity anomalies extending further to the north at the northeast portion of the study area and Bottlecap Cave to the west; (c) A view of Model 7 facing East. See the red box on Figure 3b for location. Note the cross-sectional view of Legend Cave which conforms well with the known cave length. A large increase in resistivity was observed on the north side of Legend Cave which is cut off by roof collapse.

exist, particularly to the north of Legend Cave (Fig. 10c). The presence of additional caves at similar elevations and in close proximity to one another can be expected in west-central Florida. The Dames Caves complex, located only one kilometer east of the study area, consists of several isolated caves within a few tens of meters of each other. From previous research, it appears that other shallow voids do indeed exist in the Brooksville Ridge area and elsewhere, often occurring as near-surface water table features that may have formed without entrances until subsequent sea level drop allowed their breach (Florea et al., 2007; Gulley et al., 2013).

3D Visualization

3D Site Model

Additional software is necessary to simultaneously present the 3D resistivity data and the cave geometries. The combined site model was compiled from each of the 3D block models and then imported into Voxler 3D. A relatively high range in resistivity was observed across the study area and ranged from tens to thousands of Ωm. Analysis of the ERT data along with the use of cross-over plots conducted for known cave locations indicates that the 375 Ωm contour conforms most closely to the known Legend Cave location and the 2,000 Ωm corresponds most closely to the known Bottlecap Cave location (Fig. 11a). This difference conforms to the previous observation that E−W surveys tend to show higher resistivities at cross-over points. This iso-surface plot from the 3D site model suggests potential voids at many locations and various depths, but it shows poor resolution of the mapped 3D structures.

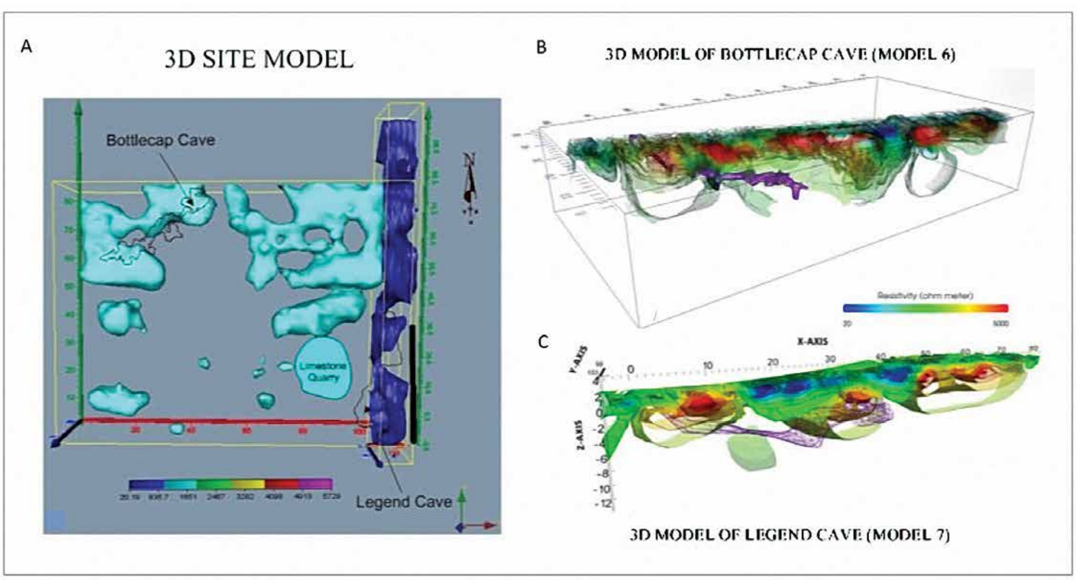

Figure 11. (a) A plan view of the 3D isosurface site model, contoured at 375 Ωm in dark blue and 2,000 Ωm in light blue. (Note the lower range in resistivity in the N-S oriented transect lines when compared to the higher resistivity range in the E-W transects); (b) shows a 3D view of Bottlecap Cave (Model 6) facing southeast. Model 6 indicates some correlation with high resistivities at the cave entrance. The deeper extent of the cave lies in a portion of the resistivity volume in which resistivities vary quite smoothly, and few iso-contours exist; (c) shows a 3D view of Legend Cave (Model 7) facing west which shows good correlation with the two larger rooms and no detection of the smaller connecting passage way.

Previous studies also noted poor results using the iso-surface plot (Chambers et al., 2012), revealing a significant limitation with this method for large scale use. A significant loss in 3D structure and resolution has also been previously noted when combining smaller subdomains (Rucker et al., 2009).

3D Cave Models

To make 3D visual comparisons between the quasi-3D ERT data with the 3D cave models, we used Paraview to render an isosurface map of the resistivity data exported from Earthimager 3D. A color map was applied using the data scales, values and range of resistivity across the site. The 3D cave models were then imported into Paraview and spatially referenced to align the cave mesh with the 3D resistivity contour model. Display settings were adjusted to allow for shading and wireframe rendering. Autodesk Maya was utilized to render the exported 3D models with more advanced features and image quality enhancements, such as lighting and transparency (Figs. 11b-c).

Figures 11b and 11c illustrate that some cave anomalies appeared interconnected where roof collapse was known and in other cases very tight passages were not detected at all. The two large northern rooms, which are connected by a small passage, are detected as one large anomaly. As seen in Figures 10b and 10c, several other highly resistive anomalies are also observed in the 3D block models, which are similar in resistivity, structure, and depth to the cave anomalies. As previously noted, these highly resistive features are suspected to be additional voids, which may suggest a series of cave passages that are not interconnected.

DISCUSSION

Overall, the findings from the 3D block models and the 3D visualization illustrate the difficulties of imaging cave geometries in eogenetic karst settings that are highly heterogeneous geomorphologically. The mapped voids presented here are only moderately complex cave structures; however, surrounding subsurface geology, consisting of near-surface clays (low resistivity, underlain by siliceous limestone (medium to high resistivity) with potentially numerous unmapped and potentially sediment-filled voids (high resistivity) appears highly variable. Thus, high matrix porosity plus disconnected voids present complexities that are often difficult to resolve using 2D and 3D ERT imaging in shallow eogenetic karst areas. Small interconnecting conduits within Legend Cave are not detected and, in some cases, large known cavities are exaggerated in size and shape. Relatively small cave features are increasingly difficult to detect with depth (Parise et al., 2015), as demonstrated for a synthetic sphere (van Nostrand and Cook, 1966). In this morphologically-diverse, eogenetic karst environment, higher data density, array geometries with higher resolution at depth, and multiple geophysical methods may clearly be desirable based on the results presented herein when attempting to detect shallow subsurface voids.

At this site, the lines in the E−W direction had a generally higher resistivity response than in the N−S direction. This could be indicative of an overall anisotropy in the resistivity, or of data sets acquired under different soil moisture conditions. However, the two elongated cave systems are not parallel, which does not indicate preferential orientation of voids at this site that would contribute to an overall anisotropy. Significantly different rainfall conditions were not noted at the time of acquisition of the N−S versus E−W trending profiles.

We also note that Legend Cave was better resolved, with lines directly overhead and in line with the cave's path, than Bottlecap Cave. The ability to resolve Bottlecap Cave significantly diminished at depth (Figure 10). This may have been a result of the slight off-set of the ERT transect lines overlying Bottlecap Cave, and highlights the importance of transect line orientation and the diminished resolvability of off-line features. Additionally, the Bottlecap Cave tablet shaped passage is significantly smaller than Legend Cave, which most likely resulted in the ERT's inability to detect the smaller cave passage. Lack of electrical current penetration at depth is particularly a problem in settings where conductive (low-resistivity) zones exist near the surface and concentrate current flow near the surface. Furthermore, with resistivity systems with a fixed number of electrodes, there is inherently a trade-off between line length, for greater depth penetration, and spatial resolution, which requires more closely spaced electrodes.

Studies have shown that water content at the time of ERT data collection can have an effect on the void resolution (Soupios et al., 2007). This is most closely related to seasonal changes in pore water during times of high and low rainfall that can influence the overall conductivity of the subsurface soils. For large scale surveys, we note that timely data collection may not always be possible. Water ponding in cave floors could make current flow pathways-and resistivity signals significantly more difficult to detect.

CONCLUSIONS

Overall, we find that quasi-3D ERT for mapping air-filled caves in the vadose zone of eogenetic karst in west-central Florida is an improvement over simple 2D profiles, but suffers several limitations of the technology. Prior to surveying, the use of a synthetic model was highly beneficial for selecting the most appropriate array geometry. The Dipole-Dipole array was determined to be an effective array for identifying complex 3D structure with little added value by combining additional arrays and, while not part of this study, the addition of a strong-gradient array may work better to identify karst features. The EarthImager L_2-norm (Smooth) inversion method provided somewhat better results when compared against the L_1-norm (Robust). This is contrary to the results of other cave studies. We would recommend trying both inversions to determine the most appropriate inversion method at a given site. The orientation of transects should also be a point of consideration as the best results in this case were obtained by profiles parallel to the strike of the cave. The 3D inversions should try to incorporate as many lines as possible in one block model (Rucker et al., 2009). This study was limited by computing access to invert the data in independent subsets. Possible use of an algorithm for faster 3D inversion of subsurface electrical resistivity data may also be beneficial in modeling larger data sets (Papadopoulos et al., 2011). In this study, line length was limited by site constraints, as clearly longer lines could have improved resolution at depth.

This study of Bottlecap and Legend Caves demonstrates the challenges of detecting the true 3D cave structure in highly variable eogenetic karst terranes. In this environment, a heterogeneous limestone with high matrix porosity and shallow cavities, the quasi-3D ERT approach was expected to provide a more accurate picture of subsurface resistivity than isolated 2D profiles. We found that 3D surveys indeed produced generally better agreement between resistivity anomalies and mapped cave locations than did isolated 2D lines. 3D visualization of the cave models indicated good resolution in the near-surface, with large cavities being detected, and diminished resolution with depth. However, a clear limitation of ERT for eogenetic karst terranes is the inability to detect smaller cavities and resolve their morphology, which may require the additional use of other geophysical methods and consideration of site-specific soil overburden and moisture conditions at the time of investigation.

ACKNOWLEDGEMENTS

Special thanks to the University of South Florida's (USF) School of Geosciences, which facilitated a collaboration of multiple disciplines including geophysics, geology, speleology, geography and environmental science. We thank Rimkus Consulting Group, Inc. for use of their electrical resistivity survey equipment; the USF Alliance for Integrated Spatial Technologies for use of their geospatial lab; and the USF Advanced Visualization Center and Research Computing for their assistance with some of the 3D rendering and visualization images presented. Thanks to Kamal Humagain and Grant Harley for assistance with cave survey of Legend Cave and Robert Brooks for assistance with Bottlecap Cave survey. Special thanks to Withlacoochee State Forest for permits and access to the study sites.

REFERENCES

Abu-Shariah, Mohammed I.I., 2009, Determination of cave geometry by using a geoelectrical resistivity inverse model: Engineering Geology, v.105, p. 239−244. https://doi.org/10.1016/j.enggeo.2009.02.006

ASTM, 1999, Standard Guide for using the Direct Current Resistivity Method for Subsurface Investigation D 6431-99.

Brinkmann, R. and Reeder, P., 1994, The influence of sea-level change and geologic structures on cave development in west-central Florida: Physical Geography v. 16, no. 1, p. 52−61. Cardarelli, E., Cercato, M., Cerreto, A., and Di Filippo, G., 2010, Electrical resistivity and seismic refraction tomography to detect buried cavities: Geophysical Prospecting, v. 58, p. 685−695. https://doi.org/10.1111/j.1365-2478.2009.00854.x

Catt, L.M.L, West, L.J., and Clark, R.A., 2009, The use of reference models from a priori data to guide 2D inversion of electrical tomography data: Geophysical Prospecting, v. 57, p. 1035−1048. https://doi.org/10.1111/j.1365-2478.2008.00774.x

Chambers, J.E., Kuras, O., Meldrum, P.I., Ogilvy, R.D., Hollands, J., 2006, Electrical resistivity tomography applied to geologic, hydrogeologic, and engineering investigations at a former waste-disposal site: Geophysics, v. 71, no. 6, p. B231−B239. https://doi.org/10.1190/1.2360184

Chambers, J.E., Wikinson, P.B., Wardrop, D., Hameed, A., Hill, I., Jeffrey, C., Loke, M.H., Meldrum, P.I., Kuras, O., Cave, M., and Gunn, D.A., 2012, Bedrock detection beneath river terrace deposits using three-dimensional electrical resistivity tomography: Geomorphology. https://doi.org/10.1016/j.geomorph.2012.03.034

Crawford, N., 1989, The Karst Landscape of Warren County: Warren County Comprehensive Plan. Bowling Green. Special Report to the City-County Planning Commission of Warren County: p. 22−41.

Crawford, N., Lewis, M., Winters, S., and Webster, J., 1999, Microgravity Techniques for Subsurface Investigations of Sinkhole Collapses and for Detection of Groundwater Flowpaths through Karst Aquifers, in *Beck, B.F., Pettit, A.J. and Herring, J.G., eds.,* Hydrology and Engineering Geology of Sinkholes and Karst, Balkema, Rotterdam, 478 p.

Dahlin, T. and Zhou, B., 2004, A numerical comparison of 2D resistivity imaging with 10 electrode arrays: Geophysical Prospecting, v. 52, p. 379−398. https://doi.org/10.1111/j.1365-2478.2004.00423.x

Doll, W.E., Nyquist, J.E., Carpenter, P.J., Kaufmann, R.D., and Carr, B.J., 1998, Geophysical Surveys of a Known Karst Feature, Oak Ridge Y-12 Plant, Oak Ridge, Tennessee, Environmental and Engineering Geophysics 3, p. 133−146 (Accessed on July 14, 2010). https://doi.org/10.2172/8046

El-Qady, G., Hafez, M., Abdalla, M.A., and Ushijima, K., 2005, Imaging Subsurface Cavities Using Geoelectric Tomography and Ground-Penetrating Radar: Journal of Cave and Karst Studies, v. 67, no. 3, p. 174−181.

Ezersky M., 2008, Geoelectric structure of the Ein Gedi sinkhole occurrence site at the Dead Sea shore in Israel: Journal of Applied Geophysics, v. 64, p. 56−69. https://doi.org/10.1016/j.jappgeo.2007.12.003

Florea, L., 2006, Architecture of air-filled caves within the karst of the Brooksville Ridge, west central Florida. Journal of Cave and Karst Studies, v. 2, no. 2, p. 64−75.

Florea, L.J., and Vacher, H.L. 2006, Springflow Hydrographs: Eogenetic vs. Telogenetic Karst: Groundwater, v. 44, no. 3, p. 352−361. https://doi.org/10.1111/j.1745-6584.2005.00158.x

Florea, L.J., Vacher, H.L., Donahue, B., and Naar, D., 2007, Quaternary cave levels in peninsular Florida: Quaternary Science Reviews, v. 26: p. 1344−1361. https://doi.org/10.1016/j.quascirev.2007.02.011

Florida Geological Survey, 2010, Florida Rocks and Minerals: http://www.dep.state.fl.us/geology/geologictopics/rocks/florida_rocks.htm#Rocks%20of%20Florida (Accessed July, 29, 2010).

Fu, Z., Ren, Z., Hua, X., Shi, Y., Chen, H., Chen, C., Li, Y., and Tang, J., 2020, Identification of underground water-bearing caves in noisy urban environments (Wuhan, China) using 3D electrical resistivity tomography techniques: Journal of Applied Geophysics, v. 174, https://doi.org/10.1016/j.jappgeo.2020.103966

Gambetta, M., Armadillo, E., Carmisciano, C., Stefanelli, P., Cocchi, L., and Tontini, C., 2011. Determining geophysical properties of a near-surface cave through integrated microgravity vertical gradient and electrical resistivity tomography measurements: Journal of Cave and Karst Studies, v. 72, no. 1, p. 11−15. https://doi.org/10.4311/jcks2009ex0091

Gary, M.O., Rucker, D.F., Smith, B.D., Smith, D.V. and Befus, K., 2013, Geophysical Investigations of the Edwards-Trinity Aquifer System at Multiple Scales: Interpreting Airborne and Direct-Current Resistivity in Karst: Proceedings of the 13th Sinkhole Conference NCKRI Symposium 2, p. 195−206.

Gharibi, M. and Bentley, L., 2005, Resolution of 3-D Electrical Resistivity Images from Inversions of 2-D Orthogonal Lines: Journal of Environmental and Engineering Geophysics, v. 10, no. 4, p. 339−349. https://doi.org/10.2113/JEEG10.4.339

Gibson, P.J., Lyle, P., and George, D.M., 2004, Applications of resistivity and magnetometry geophysical techniques for near-surface investigations in karstic terranes in Ireland. Journal of Cave and Karst Studies, v. 66, no. 2, p. 35−38.

Gulley, J. D., Martin, J. B., Moore, P. J. and Murphy, J., 2013, Formation of phreatic caves in an eogenetic karst aquifer by CO_2 enrichment at lower water tables and subsequent flooding by sea level rise: Earth Surface Processes and Landforms, v. 38, p. 1210–1224. https://doi.org/10.1002/esp.3358

Häuselmann, P. (ed.), 2010, UIS Mapping Grades: Survey and Mapping Working Group, UIS Informatics Commission, Version 1.

Jackson, P.D., Earl, S.J., and Reece, G.J., 2001, 3D resistivity inversion using 2D measurements of the electric field: Geophysical Prospecting, v. 49, p. 26−39. https://doi.org/10.1046/j.1365-2478.2001.00241.x

Jenson, J.W., Keel, T.M., Mylroie, J.R., Mylroie, J.E., Stafford, K.W., Taborosi, D., and Wexel, C., 2006, Karst of the Marian Islands: The interaction of tectonics, glacio-eustasy, and freshwater/seawater mixing in island carbonates, in Harmon, R.S., Wicks, C.M., Ford, D.C, and White, W.B. eds., Perspectives on Karst Geomorphology, Hydrology, and Geochemistry: Geological Society of America, Special Paper 404. https://doi.org/10.1130/2006.2404(11)

Kambesis, P.N., Larson, E.B., Mylroie, J.E., 2015, Morphometric analysis of cave patterns using fractal indices, in Feinberg, J., Gao, Y., and Alexander, E.C., Jr., eds., Caves and Karst Across Time: Geological Society of America Special Paper, 516, p. 1–20. https://doi.org/10.1130/SPE516

Kaufmann, G., Romanov, D., and Nielbock, R., 2011, Cave detection using multiple geophysical methods: Unicorn cave, Harz Mountains, Germany: Geophysics, v. 76, no. 3, p. B71−B77. https://doi.org/10.1190/1.3560245

Kaufmann, O., Deceuster, J., and Quinif, Y., 2012, An electrical resistivity imaging-based strategy to enable site-scale planning over covered paleokarst features in the Tournaisis area (Belgium): Engineering Geology, v. 133-134, p. 49−65. https://doi.org/10.1016/j.enggeo.2012.01.017

Kirk, G.K., 1981, Handbook of geophysical cavity-locating techniques with emphasis on electrical resistivity, U.S. Department of Transportation Federal Highway Administration, Environmental Exploration, U.S. Government Printing Office, HP, Morgantown, 175.

Kruse, S., Grasmueck, M., Weiss, M., and Viggiano, D., 2006, Sinkhole structure imaging in covered Karst terrain: Geophysical Research Letters, v. 33: L16405. https://doi.org/10.1029/2006GL026975

Lace, M. and Mylroie, M., 2013, Coastal Cave and Karst Resource Management, in Lace, M. and Mylroie, M., eds., Coastal Karst Landforms, v. 5, p. 127−143. https://doi.org/10.1007/978-94-007-5016-6_6

Land, L. and G. Veni, 2012, Electrical resistivity surveys of anthropogenic karst phenomena, southeastern New Mexico, New Mexico: Geology, v. 34, p. 117−125.

Leucci G., Parise M., Sammarco M., and Scardozzi G., 2016, The use of geophysical prospections to map ancient hydraulic works: the Triglio underground aqueduct (Apulia, Southern Italy): Archaeological Prospection, v. 23, p. 195−211. https://doi.org/10.1002/arp.1541

Loke, M.H. and Barker, R.D., 1996a, Rapid least-squares inversion of apparent resistivity pseudosections by a quasi-Newton method: Geophysical Prospecting, v. 44, p. 131−152. https://doi.org/10.1111/j.1365-2478.1996.tb00142.x

Loke, M.H. and Barker, R.D., 1996b, Practical techniques for 3D resistivity surveys and data inversion: Geophysical Prospecting, v. 44, p. 499−523. https://doi.org/10.1111/j.1365-2478.1996.tb00162.x

Loke, M.H., Chambers, J.E., Rucker, D.F., Kuras, O. and Wilkinson, P.B., 2013, Recent developments in the direct-current geoelectrical imaging method: Journal of Applied Geophysics, v. 95, p. 135−156. https://doi.org/10.1016/j.jappgeo.2013.02.017

Majzoub, A.F., Stafford, K.W., Brown, W.A., and Ehrhart, J.T., 2017, Characterization and delineation of gypsum karst geohazards using 2D electrical resistivity tomography in Culberson County, Texas, USA: Journal of Environmental and Engineering Geophysics, v. 22, p. 411−420. https://doi.org/10.2113/JEEG22.4.411

Martorana, R., Fiandaca, G., Casas Ponsati, A., and Cosentino, P.L., 2009, Comparative tests on different multi-electrode arrays using models in near-surface geophysics: Journal of Geophysics and Engineering, v. 6, p. 1−20. https://doi.org/10.1088/1742-2132/6/1/001

Margiotta S., Negri S., Parise M., and Valloni R., 2012, Mapping the susceptibility to sinkholes in coastal areas, based on stratigraphy, geomorphology and geophysics: Natural Hazards, v. 62, no. 2, p. 657−676. https://doi.org/10.1007/s11069-012-0100-1

McCormack, T., O'Connell, Y., Daly, E., Gill, L.W., Henry, T., and Perriquet, M., 2017, Characterisation of karst hydrogeology in Western Ireland using geophysical and hydraulic modelling techniques: Journal of Hydrology: Regional Studies, v. 10, p. 1−17. https://doi.org/10.1016/j.ejrh.2016.12.083

Miller, Benjamin V., 2010, Cave map of Bottlecap Cave, Citrus County, Florida, unpublished, Florida Speleological Survey.

Mohamed, A.M.E., El-Hussain, I., Deif, A., Araffa, S.A.S., Mansour, K., and Al-Rawas, G., 2019, Integrated ground penetrating radar, electrical resistivity tomography and multichannel analysis of surface waves for detecting near-surface caverns at Duqm area, Sultanate of Oman: Near Surface Geophysics, v. 17. https://doi.org/10.1002/nsg.12054

Nasseri-Moghaddam, A., Cascante, G., and Hutchinson, J., 2005, A New Quantitative Procedure to Determine the Location and Embedment Depth of a Void Using Surface Waves: Journal of Environmental and Engineering Geophysics, v. 10, no. 1, p. 51−64. https://doi.org/10.2113/JEEG10.1.51

Nazaruddin, D. A., Amiruzan, Z. S., Hussin, H., & Jafar, M. T. M., 2017, Integrated geological and multi-electrode resistivity surveys for groundwater investigation in Kampung Rahmat village and its vicinity, Jeli district, Kelantan, Malaysia: Journal of Applied Geophysics, v. 138, p. 23−32. https://doi.org/10.1016/j.jappgeo.2017.01.012

Neyamandpour, A., Taib, S., and Wan Absullah, W.A.T., 2009, An Application of Three-Dimensional Electrical Resistivity Imaging for the Detection of an Underground Waste-Water System: Studia Geophysica et Geodaetica, v. 53, p. 389−402. https://doi.org/10.1007/s11200-009-0027-5

Neyamandpour, A., Wan Absullah, W.A.T., Taib, S., and Neyamadpour, B., 2010, Comparison of Wenner and dipole-dipole arrays in the study of an underground three-dimensional cavity. Journal of Geophysics and Engineering, v. 7, p. 30−40. https://doi.org/10.1088/1742-2132/7/1/003

Palmer, A.N., 2007, Cave Geology, Dayton, Ohio: Cave Books.

Pánek, T., Margielewski, W., Taborik, P., Urban, J., Hradecky, J., and Szura, C., 2010, Gravitationally induced caves and other discontinuities detected by 2D electrical resistivity tomography: Case studies from the Polish Flysch Carpathians: Geomorphology, v. 123, p. 165−180. https://doi.org/10.1016/j.geomorph.2010.07.008

Papadopoulos, N.G., Tsourlos, P., Tsokas, G.N., and Sarris, A., 2006, Two-dimensional and Three-dimensional Resistivity Imaging in Archeological Site Investigation: Archaeological Prospection, v. 13, p. 163−181. https://doi.org/10.1002/arp.276

Papadopoulos, N.G., Yi, M., Kim, J. Tsourlos, P., and Tsokas, G. N., 2010, Geophysical investigation of tumuli by means of surface 3D Electrical Resistivity Tomography: Journal of Applied Geophysics, v. 70, p. 192−205. https://doi.org/10.1016/j.jappgeo.2009.12.001

Pánek, T., Margielewski, W., Taborik, P., Urban, J., Hradecky, J., and Szura, C., 2010, Gravitationally induced caves and other discontinuities detected by 2D electrical resistivity tomography: Case studies from the Polish Flysch Carpathians. Geomorphology, v. 123, p. 165−180. https://doi.org/10.1016/j.geomorph.2010.07.008

Parise, M., and Gunn, J., (eds.), 2007, Natural and anthropogenic hazards in karst areas: Recognition, Analysis and Mitigation: Geological Society London, sp. publ. 279. https://doi.org/10.1144/SP279.1

Parise M., Closson D., Gutierrez F., and Stevanovic Z., 2015, Anticipating and managing engineering problems in the complex karst environment: Environmental Earth Sciences, v. 74, 7823−7835. https://doi.org/10.1007/s12665-015-4647-5

Polk, J.S., 2009, Proxy Records of Climate Change in Subtropical and Tropical Karst Environments, [Ph.D. Dissertation]: Tampa, University of South Florida.

Polk, J.S., 2012, Legend Cave Map, unpublished, Withlacoochee State Forest, Citrus, County, Florida.

Polk, J.S., van Beynen, P.E., and Wynn, J.G., 2012, An Isotopic Calibration Study of Precipitation, Cave Dripwater, and Climate in West-central Florida: Hydrological Processes. https://doi.org/10.1002/hyp.8169

Prins, C., Thuro, K., Krautblatter, M., Schulz, R., 2019, Testing the effectiveness of an inverse Wenner-Schlumberger array for geoelectrical karst void reconnaissance, on the Swabian Alb high plain, new line Wendlingen–Ulm, southwestern Germany: Engineering Geology, v. 249, p. 71−76. https://doi.org/10.1016/j.enggeo.2018.12.014

Redhaounia, B., Ilondo, B. O., Gabtni, H., Sami, K., and Bédir, M., 2016, Electrical Resistivity Tomography (ERT) applied to Karst carbonate aquifers: case study from Amdoun, northwestern Tunisia: Pure and Applied Geophysics, v. 173, no. 4, 1289−1303. https://doi.org/10.1007/s00024-015-1173-z

Redhaounia, B., Bédir, M., Gabtni, H., Batobo, O. I., Dhaoui, M., Chabaane, A., and Khomsi, S., 2016, Hydro-geophysical characterization for groundwater resources potential of fractured limestone reservoirs in Amdoun Monts (North-western Tunisia): Journal of Applied Geophysics, v. 128, 150−162. https://doi.org/10.1016/j.jappgeo.2016.03.005

Roth, M.J.S., Mackey, J.R., Mackey, C., and Nyquist, J.E., 2002, A case study of the reliability of the multielectrode earth resistivity testing for geotechnical investigations in karst terrains: Engineering Geology, v. 65, p. 225−232. https://doi.org/10.1016/S0013-7952(01)00132-6

Rucker, D.F., Levitt, M.T., and Greenwood, W.J., 2009, Three-dimensional electrical resistivity model of a nuclear waste disposal site: Journal of Applied Geophysics, v. 69, p. 150−164. https://doi.org/10.1016/j.jappgeo.2009.09.001

Schoor, M.V., 2002, Detection of sinkholes using 2D electrical resistivity imaging: Journal of Applied Geophysics, no.50, p. 393−399. https://doi.org/10.1016/S0926-9851(02)00166-0

Schrott, L., and Sass, O., 2008, Application of field geophysics in geomorphology: Advances and limitations exemplified by case studies: Geomorphology, v. 93, p. 55−73.

Scott, T.M., 1997, Miocene to Holocene History of Florida. In: Randazzo, A.F., Jones, D.S. (Ed.) The Geology of Florida, University Press of Florida, Gainesville, p. 57−67. https://doi.org/10.1016/j.geomorph.2006.12.024

Scott, T.M., 2001, The Geologic Map of Florida: Florida Geological Survey Report 80.

Sheehan, J.R., Doll, W.E., and Watson, D.B., 2005, Detecting Cavities with Seismic Refraction Tomography: Can it be done? Extended abstract, presented at the 2005 Annual Meeting of the Symposium on the Application of Geophysics to Engineering and Environmental Problems, Atlanta, GA, April 307, 2005. https://doi.org/10.4133/1.2923557

Sinclair, W.C., Stewart, J.W., Knutilla, R.L., Gilboy, A. E., and Miller, R.L., 1985, Types, Features, and Occurrence of Sinkholes in the Karst of West-central Florida: US Geological Survey, Water Resources Investigations Report, 85-4126.

Soupios, P.M., Georgakopoulos, P., Papadopoulos, N., Saltas, V., Andreadakis, A., Vallianatos, F., Sarris, A., and Makris, J.P., 2007, Use of engineering geophysics to investigate a site for a building foundation: Journal of Geophysics and Engineering, v. 4, p. 94−103. https://doi.org/10.1088/1742-2132/4/1/011

Southwest Florida Water Management District, 2006, Lidar data acquired from http://www.swfwmd.state.fl.us/data/

Sumanovac, F and Weisser, M., 2001, Evaluation of resistivity and seismic methods for hydrogeological mapping in karst terrains: Journal of Applied Geophysics, v.47, p. 13−28. https://doi.org/10.1016/S0926-9851(01)00044-1

Torrese, P., 2020, Investigating karst aquifers: Using pseudo 3-D electrical resistivity tomography to identify major karst features: Journal of Hydrology, v. 580. https://doi.org/10.1016/j.jhydrol.2019.124257

Vacher, L. and Mylroie, J., 2002, Eogenetic Karst from the Perspective of an Equivalent Porous Medium: Carbonates and Evaporites, v.17, no. 2, p. 182−196. https://doi.org/10.1007/BF03176484

Van Nostrand, R.G. and Cook, K.L., 1966, Interpretation of Resistivity Data: Geological Survey Professional Paper 499. United States Government Printing Office, Washington. https://doi.org/10.3133/pp499

Wilkinson, P.B., Chambers, J. E., Meldrum, P.I., Ogilvy, R.D., Mellor, C.J., and Caunt, S., 2005, A Comparison of Self-Potential Tomography with Electrical Resistivity Tomography for the Detection of Abandoned Mineshafts: Journal of Environmental and Engineering Geophysics, v.10, no. 4, p. 381−389. https://doi.org/10.2113/JEEG10.4.381

Xia, J. and Miller, R.D., 2007, Integratred geophysicial survey in defining subsidence on a golf course: Journal of Geophysics and Engineering, v.4, p. 443−451. https://doi.org/10.1088/1742-2132/4/4/010

Zhou, W. and Beck B.F., 2011, Engineering issues on karst: In: P. van Beynen (Ed), Karst Management. Springer, Dordrecht, p. 9−45. https://doi.org/10.1007/978-94-007-1207-2_2

Zhu, J., Currens, J. C. and Dinger, J. S., 2011, Challenges of using electrical resistivity method to locate karst conduits-A field case in the Inner Bluegrass Region, Kentucky: Journal of Applied Geophysics, v.75, p. 523−530. https://doi.org/10.1016/j.jappgeo.2011.08.009